$B^0 \to \mu^+\mu^-$ and $B_s^0 \to \mu^+\mu^-$ Studies at the LHCb Experiment

Hannah Evans

July 1, 2014

Abstract

The search for $B^0 \to \mu^+\mu^-$ and $B_s^0 \to \mu^+\mu^-$ is being carried out at the LHCb experiment. The latest it has produced measurements are $\mathcal{B}(B_s^0 \to \mu^+\mu^-) = (2.9^{+1.1}_{-1.0}) \times 10^{-9}$ and $\mathcal{B}(B^0 \to \mu^+\mu^-) < 7.4 \times 10^{-10}$ at 95% C.L. This report focuses on improvements in the signal selection efficiency for future analyses and improvements in mass reconstruction resolution.

Contents

1 Introduction

The LHC machine operates at the forefront of particles physics experiments. The decays $B_s^0 \to \mu^+\mu^-$ and $B^0 \to \mu^+\mu^-$ have been studied at many different experiments and are currently being studied at the LHCb experiment at the LHC. The branching fractions for these decays offer tight constraints for new physics models.

Currently the LHC is in scheduled downtime, this report outlines several studies which look to improve the $\mathcal{B}(B_s^0 \to \mu^+\mu^-)$ analysis for future data runs. The LHC machine is described in Section 2 and Section 3 introduces the LHCb experiment. The Standard Model and theory behind $B_s^0 \to \mu^+\mu^-$ is outlined in Section 4, along with the current status of searches for $\mathcal{B}(B_s^0 \to \mu^+\mu^-)$. Section 5 details studies aimed at improving signal selection efficiencies by looking at efficiencies of the stripping selection and Section 6 describes improvements to the resolution of the mass reconstruction. Finally Section 7 briefly outlines possible future work.

2 The LHC

The Large Hadron Collider (LHC) [1] is a two beams collider predominately designed to collide protons at an energy of 14 TeV but the accelerator can also study collisions of heavy ions. It has been built on the Franco-Swiss border in the tunnel previously used for the LEP machine at CERN[1] with the aim of studying predictions of the Standard Model of particle physics and looking for New Physics beyond the Standard Model. The LHC is the last element of an accelerator complex shown in Fig. 1: accelerators previously used at CERN have been modified in order to supply the LHC with high density proton bunches. Protons are first accelerated in the Linac 2 to an energy of 50MeV, the then pass through the Proton Synchrotron Booster, Proton Synchrotron and the Super Proton Synchrotron reaching and energy of 450 GeV before injection into the LHC where they are accelerated up to final energy.

The LHC began taking data in December 2009, most of the data has been acquired during the runs in 2011 and 2012 at center of mass energies of 7 TeV and 8 TeV, respectively, with 50 ns between proton bunches. It is currently in downtime undergoing upgrades and shall resume operation 2015 colliding proton bunches with a spacing of 25 ns at a center of mass energy of 13 TeV.

There are four detectors at the LHC, ATLAS, CMS, ALICE and LHCb, placed where the two beams cross over. The ATLAS [2] and CMS [3] detectors are general purpose detectors with 4π angular acceptance and have been designed to perform general searches for New Physics and the Higgs boson.[2] The ALICE [6] detector is specialised to study heavy ion collisions in order to investigate strongly interacting matter and quark-gluon plasmas. The LHCb [7] detector is a single-arm spectrometer designed for the study of B-hadron decays.

3 The LHCb

The LHCb detector is designed specifically to study CP violation and rare decays of b-hadrons and c-hadrons building on work done a the B factories and the Tevatron. At the high energies the LHC operates at $b\bar{b}$ pairs are produced together at low polar angles in either the forwards or backwards cone along the beam direction. The detector is designed as a single-arm spectrometer to take advantage of this behaviour.

A cross-section of the detector layout is shown in Fig. 2.

The LHCb detector is composed of sub-detectors with different design purposes. The vertex locator (VELO) and the tracking stations (TT, T1, T2 and T3) are key for tracking charged particles travelling through the detector. The RICH detectors, calorimeters (ECAL, HCAL, PS

[1] CERN is the European Organisation for Nuclear Research.

[2] ATLAS and CMS both discovered a possible candidate for the Standard Model Higgs in 2013 [4, 5].

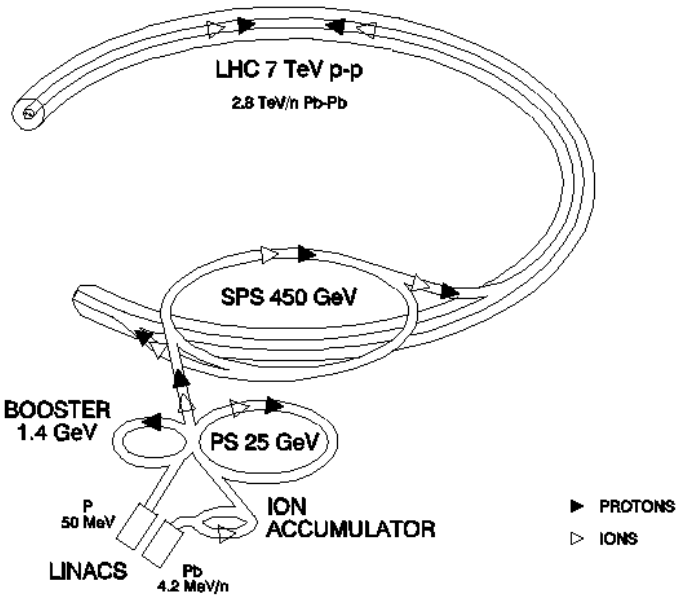

Figure 1: The LHC and adjoining accelerator chain at CERN [1]

and SPD) and the muon stations (M1-5) are necessary for particle identification. The dipole magnet in the detector is used alongside the tracking stations in order to measure particle charge and momentum.

The VELO is the tracking detector closest to the interaction point. It is designed to locate primary and secondary decay vertices. Secondary vertices occur within the VELO due to the short lifetime of b-hadrons, whereas primary vertices do not occur in the VELO but tracks in the VELO are extrapolated backwards to determine the vertex location. The VELO is a silicon micro-strip detector which give good resolution of tracks and decay vertices.

The T1-3 tracking station consist of the Inner Tracker (IT) and the Outer Tracker (OT). The IT is a silicon micro-strip detector and makes up the inner sections of the stations closest to the beam pipe. The OT is a straw-tube drift-chamber and covers the outer sections of the T1-3 stations. Silicon micro-strip detectors are needed in the IT due to high particle occupancy however the particle flux is lower at large polar angles from the beam pipe allowing straw tubes to be used in the OT as the occupancy is lower. The Tracker Turicensis (TT) is also a silicon micro-strip detector upstream of IT and OT, it spans the full acceptance of the LHCb detector. The TT, IT and OT work together with the dipole magnet to measure charge and momentum of particles travelling through the detector. Obtaining good momentum resolution is vital because the momentum resolution directly affect the invariant mass resolution of reconstructed particles.

Distinguishing between e, μ, p, K, π and photons is important for accurately reconstructing particle decays. Each sub-detector related to particle identification is specialised for different particles. The sub-detectors for particle identification are the two RICH detectors, the Preshower detector (PS), Scintillating Pad Detector (SPD), the electromagnetic calorimeter (ECAL), the hadronic calorimeter (HCAL) and the muon tracking stations (M1-5).

The particle identification detectors closest to the interaction point are the RICH 1 and RICH 2. These detectors are ring imaging Čerenkov detectors, designed to separate charged pions and kaons which are produced in large number from b-hadron decays. In LHCb, high momentum particles are produced at small polar angles and lower momentum particles at larger polar angles, therefore two RICH detectors are needed to cover the full momentum and acceptance range. The RICH 1 is composed of an areogel and C_4F_{10} gas radiator, it is sensitive to particles with momentum between 1 and 60 GeV/c. The RICH 2 is a CF_4 gas radiator and is

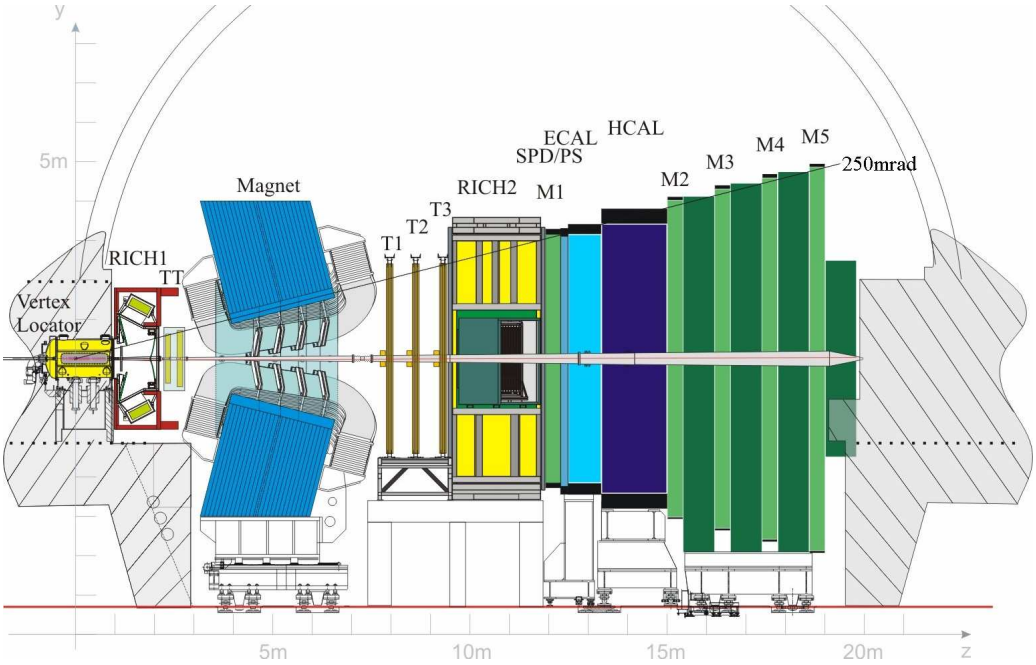

Figure 2: Cross-section of the LHCb detector the the z-axis is along the beam pipe and the y-axis is the vertical direction [7].

sensitive to particles with momentum between 15 and 100 GeV/c.

The SPD distinguishes charged and neutral particles such as photons and electrons which leave the same signals in the ECAL. The PS detector distinguishes electrons and charged pions by utilising their different interaction lengths in matter.

Downstream of the SPD and the PS is the ECAL, a lead-scintillator sampling detector. Electrons and photons interact within the lead producing electromagnetic showers, the scintillator absorbs photons produced by the showers and emits photons at different wavelengths so that photomultiplier tubes detect them. The energy of an incident particle is measured from the energy of the shower which is proportional to the light produced in the shower. Showers produced by photons can be distinguished from those produced by electrons because photons leave no hits in the tracking detectors or the SPD. Hadrons will pass though the ECAL to be detected by the HCAL. The HCAL is composed of lead and scintillator tiles and measure the energy hadronic showers produced inside it. The HCAL works in the same way as the ECAL however the lead absorber is more suited to producing hadronic showers rather than electromagnetic ones.

Muon identification is key for the analysis of several important CP violating decays and rare decays, including $B_s \to \mu^+\mu^-$. The ECAL and the HCAL absorb most particles produced in collisions. However, the high penetration power of muons allows then to pass through the ECAL and HCAL therefore the muon stations can be the in furthest part of the detector. The muon stations are multi-wire proportional chambers except the inner part of the M1 station which is a gas electron multiplier due to the high particle occupancy.

Muon identification is not only important for offline analysis but, together with information from the ECAL and HCAL, the muon system triggers events which are saved for offline analysis. The LHCb has been designed to operate at a lower instantaneous luminosity than the running of the LHC, the trigger takes the 10 MHz of data visible in the LHCb and reduces it to 5 kHz which can be stored offline. There are two levels to the trigger the Level 0 (L0) and the High Level Trigger (HLT). The L0 operates at the same time as the bunch crossings and reduced the rate to 1 MHz by using transverse momentum information from the ECAL, HCAL and the muon stations. The HLT further reduces the rate to 5 kHz, running asynchronously with the bunch crossings on a processor farm. The HLT takes events that have been triggered by the L0

and confirms them by reconstructing the events more fully using information from the VELO and other tracking stations. Once the data has been stored there are further offline selections which aim to further reduce the background and enhance the signal for particular decays. The trigger is optimised so when it is combined with the offline selection it can give the best signal and best background rejection. Since the LHCb studies many different decays there are various different triggers that are used for different analyses.

4 $B_s^0 \to \mu^+\mu^-$

The weak decays $B^0_{(s)} \to \mu^+\mu^-$ occur via flavour changing neutral currents (FCNC) in the Standard Model and are highly suppressed.

$B^0_s \to \mu^+\mu^-$ was outlined as one of six important studies to be done at the LHCb [8] due to the sensitivity of the branching fraction to contributions from new physics models. Previously these rare decays have been studied at B factories and the Tevatron, and the current measurements for the branching fractions from the LHCb are $\mathcal{B}(B^0_s \to \mu^+\mu^-) = (2.9^{+1.1}_{-1.0}) \times 10^{-9}$ at 4.0 σ significance and $\mathcal{B}(B^0 \to \mu^+\mu^-) < 7.4 \times 10^{-10}$ at 95% CL.

In this section I shall introduce the Standard Model (Section 4.1) and outline how $B^0_{(s)} \to \mu^+\mu^-$ occurs within the Standard Model (Section 4.2). The calculation of the branching fractions for the decays is explained (Section 4.3) and finally, the current status for the search and measurements of $B^0_{(s)} \to \mu^+\mu^-$ reviewed and future aims at the LHCb (Section 4.5).

4.1 The Standard Model

The Standard Model (SM) is a quantum field theory which describes matter and its interactions at a fundamental level. In the SM there are 12 fundamental spin-$\frac{1}{2}$ fermions; six quarks and six leptons. The six quarks form three families; up and down, strange and charm, top and bottom. Quarks have both electric and colour charge and combine into composite particles either as a quark anti-quark pair to make a meson or as three quarks to make a baryon.[3] Similarly leptons form three families each containing a charged and a neutral particle: e^- and ν_e, μ^- and ν_μ, τ^- and ν_τ, however leptons have no colour charge.

Quarks and leptons interact through the strong force, weak force and electromagnetic force. The strong force is described by a symmetry group of $SU(3)_C$ colour charge, quarks are the only coloured particles therefore the strong force acts only between quarks and anti-quarks. The strong force is mediated by 8 massless coloured gluons and its strength increases as distance between quarks increases.

The electromagnetic force describes interactions between electrically charged particles. The gauge boson mediating the electromagnetic force is the photon, since the photon is massless the force has in infinite range. The weak force allows interactions between all fermions in the SM, it allows flavour changing to occur between quarks or between charged leptons and their associated neutrinos. These interactions are mediated by massive gauge bosons; the $W^\pm$ and the Z^0. The weak and electromagnetic forces can be unified into a $SU(2) \otimes U(1)$ symmetry group. However is a broken symmetry because the gauge bosons have different masses for the two interactions. The Higgs mechanism accounts for this symmetry breaking, interactions of the electroweak bosons with the Higgs field causes symmetry breaking creating the massive $W^\pm$ and Z^0 and the massless photon.

The SM has evolved over time into what it is today, with discoveries prompting new theories and theoretical predictions motivation experimental searches. All fermions and bosons predicted in the SM have been discovered, the latest of these being the Higgs boson for which the ATLAS

[3]The Z(4430) is neither a meson or a baryon, it was first observed at Belle [9] and recently confirmed at the LHCb [10] with a high statistical significance. It is composed of four quarks and is the the first exotic particle to be observed at a high statistical significance.

and CMS experiments discovered a possible candidate in 2013 [4, 5]. However there are several shortcomings of the SM and observed phenomena that it does not explain, a few examples are outlined below;

- matter anti-matter asymmetry - as the universe was created matter and anti-matter would have been created in equal amounts, however the universe today is matter dominated. One process that can cause this asymmetry is CP violation, this effect enters the SM via the CKM matrix, however the effect is too small to account for the observed imbalance.
- neutrinos have been observed to oscillate [11–13], in order for neutrinos to oscillate they must be massive particles but in the SM neutrinos are massless. However the SM can be adapted to include massive neutrinos without any fundamental changes.
- gravity is not explained by the SM
- astronomical observations have revealed that the rotational speed of galaxies does not match up with the speed expect from the amount of matter visible in the universe [14–16]. If General Relativity is correct then there must be invisible matter which interacts via gravity to produce the extra mass. There is no candidate to explain this dark matter in the SM.

Therefore despite the successes of the SM there must be New Physics beyond the SM that will explain its shortcomings.

4.2 $B^0_{(s)} \to \mu^+\mu^-$ in the Standard Model

$B^0_s \to \mu^+\mu^-$ and $B^0 \to \mu^+\mu^-$ occur by flavour changing neutral currents (FCNC), they are highly suppressed decays in which quark flavour but not quark charge change. Flavour changes in quarks are allowed in the SM via the CKM matrix. The CKM matrix relates mass and flavour quark eigenstates

$$\begin{pmatrix} d' \\ s' \\ b' \end{pmatrix} = \begin{pmatrix} V_{ud} & V_{us} & V_{ub} \\ V_{cd} & V_{cs} & V_{cb} \\ V_{td} & V_{ts} & V_{tb} \end{pmatrix} \begin{pmatrix} d \\ s \\ b \end{pmatrix}$$

where the amplitude for an up quark to change flavour to a bottom quark is proportional to the CKM matrix element $|V_{ub}|^2$. The numerical magnitudes of the CKM matrix elements are given in Eq. (1) [17], it is clear that some flavour changes are probably than other, e.g. a bottom quark will change into a top quark with a much greater amplitude than to any other quark.

$$V_{CKM} = \begin{pmatrix} 0.97427 \pm 0.00015 & 0.22534 \pm 0.00065 & 0.00351^{0.00015}_{-0.00014} \\ 0.22520 \pm 0.00065 & 0.97344 \pm 0.00016 & 0.0412^{0.0011}_{-0.0005} \\ 0.00867^{+0.00029}_{-0.00031} & 0.0404^{+0.0011}_{-0.0005} & 0.999146^{+0.000021}_{-0.000046} \end{pmatrix} \quad (1)$$

All interactions in the CKM matrix are mediated by $W^\pm$, and are flavour and charge changing. The decays $B^0_s \to \mu^+\mu^-$ and $B^0 \to \mu^+\mu^-$ do not change charge and therefore cannot occur at tree level. A $\mu^+\mu^-$ pair can be produced from a Z^0, γ or H^0 which the constituent quarks of the B^0 and B^0_s cannot create. Therefore these decays occur via loop diagram such as Z^0 penguins or box diagrams. Figure 3 shows the dominant Feynman diagrams for $B^0_s \to \mu^+\mu^-$ and $B^0 \to \mu^+\mu^-$. The intermediate quark in the loop diagrams is the top quark, contributions from other quarks are negligible due to very small coupling to the b quark in the CKM matrix.

The decays $B^0_s \to \mu^+\mu^-$ and $B^0 \to \mu^+\mu^-$ are not only suppressed because they are FCNC events they are also suppressed by a factor of

$$\left(\frac{m_\mu}{m_{B^0_{(s)}}} \right)^2$$

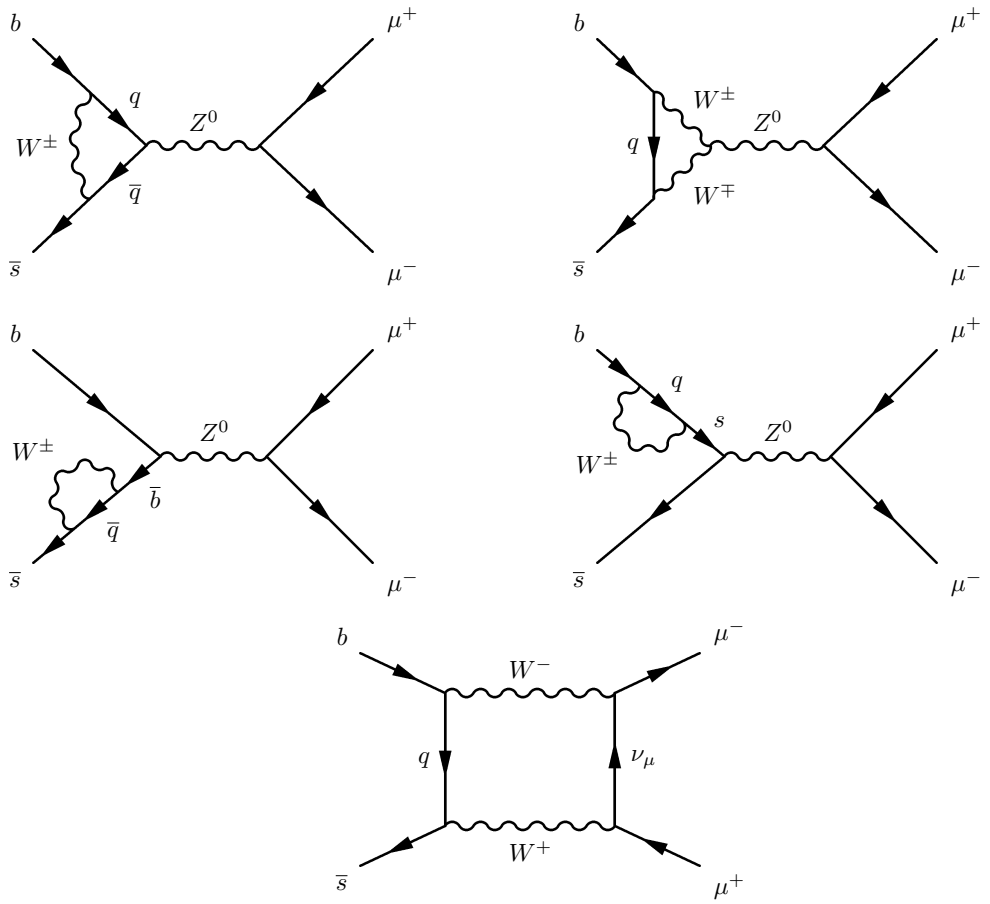

Figure 3: Feynman diagrams dominant in the SM for $B_s^0 \to \mu^+\mu^-$ [18].

due to helicity. The B hadron has zero spin therefore requiring the muons to have the same helicity.

4.3 Branching Fraction of $B^0_{(s)} \to \mu^+\mu^-$

Weak decays such as $B^0_{(s)} \to \mu^+\mu^-$, can be described using a quantum field theory technique known at the Operator Product Expansion (OPE) [19,20] to produce an effective Hamiltonian. The effective Hamiltonian divides the process into interactions on different distance scales and has the following form [21]

$$H_{eff} = \frac{G_F}{\sqrt{2}} \sum_i V^i_{CKM} \mathcal{C}(\mu)_i \mathcal{Q}(\mu)_i$$

where G_F is the Fermi constant, $\mathcal{C}(\mu)_i$ are Wilson coefficients and $\mathcal{Q}(\mu)_i$ are local operators. The energy scale μ separates the interaction into two distance scales. Wilson coefficients describe short scale processes, for energies greater than μ, they incorporate contributions from internal loops and subsequently depend on $W^\pm$, Z^0, H^0 and top quark masses. Perturbation theory can be used to calculate Wilson coefficients due to asymptotic freedom in QCD. The local operators $\mathcal{Q}_i$ describe long distance processes at energies smaller than μ, they link initial and final decay states. These operators cannot be computed using perturbation theory and therefore have the greatest theoretical uncertainty in the in the Hamiltonian in many weak hadron decays. The final Hamiltonian must be independent of μ because it is given an arbitrary size, often chosen as the mass of the decaying particle.

The effective Hamiltonian is a useful formalism for studying effects of new physics on weak decay because new physics contributions can enter the Hamiltonian though Wilson coefficients.

For the decays $B^0_s \to \mu^+\mu^-$ and $B^0 \to \mu^+\mu^-$ the effective Hamiltonian can be written as in [22]

$$H_{eff} = -\frac{4G_F}{\sqrt{2}} V_{tb}V^*_{tq} \left[\sum_{i=1}^{10} \mathcal{C}_i\mathcal{Q}_i + \mathcal{C}_P\mathcal{Q}_P + \mathcal{C}_S\mathcal{Q}_S + \mathcal{C}'_P\mathcal{Q}'_P + \mathcal{C}'_S\mathcal{Q}'_S \right] \tag{2}$$

where q corresponds to the other composite quark of B-hadron depending on whether is it B^0 or B^0_s being considered in the Hamiltonian. The terms proportional to $V_{tb}V^*_{uq}$ and $V_{cb}V^*_{cq}$ are omitted from H_{eff} because their contribution is negligible compared to the CKM couplings to the top quark.

The only operators that have non-zero contributions in the decay amplitude for $B^0_{(s)} \to \mu^+\mu^-$ are

$$\mathcal{Q}_{10} = \frac{e^2}{16\pi^2}(\bar{q}\gamma^\mu P_L b)(\bar{l}\gamma_\mu\gamma_5 l) \tag{3}$$

$$\mathcal{Q}_S = \frac{e^2}{16\pi^2} m_b(\bar{q}P_R b)(\bar{l}l) \tag{4}$$

$$\mathcal{Q}_P = \frac{e^2}{16\pi^2} m_b(\bar{q}P_R b)(\bar{l}\gamma_5 l) \tag{5}$$

$$\mathcal{Q}'_S = \frac{e^2}{16\pi^2} m_q(\bar{q}P_L b)(\bar{l}l) \tag{6}$$

$$\mathcal{Q}'_P = \frac{e^2}{16\pi^2} m_q(\bar{q}P_L b)(\bar{l}\gamma_5 l) \tag{7}$$

all other operators in equation (2) are zero due to the leptonic final states in $B^0_{(s)} \to \mu^+\mu^-$.

The dominant contribution in the SM Hamiltonian come from $\mathcal{C}_{10}$ which contains the contributions from Z^0 penguins and W-box diagrams. Contributions from $\mathcal{C}_{\mathcal{S}}$ and $\mathcal{C}_{\mathcal{P}}$, corresponding to Higgs-penguins, are negligible in the SM and can be ignored. However these contributions can be substantially increased by new physics processes. The branching fraction can therefore be written as [18]

$$\mathcal{B}(B_{(s)} \to \mu^+\mu^-) = \frac{G_F^2\alpha^2}{16\pi^3 \sin^4(\theta_W)}|V_{tb}V_{tq}^*|^2 \tau_{B_{(s)^0}} m_{B_{(s)^0}} f_{B_{(s)^0}}^2 m_\mu^2 \sqrt{1 - \frac{4m_\mu^2}{m_{B_{(s)^0}}^2}}\mathcal{C}_{10}^2$$

where $f_{B_{(s)^0}}$ is the B-hadron decay factor, $\tau_{B_{(s)^0}}$ it's lifetime and $m_{B_{(s)^0}}$ it's mass. The SM predictions for the branching fractions are [23]

$$\mathcal{B}(B_s^0 \to \mu^+\mu^-) = (3.65 \pm 0.23) \times 10^{-9}$$

$$\mathcal{B}(B^0 \to \mu^+\mu^-) = (1.06 \pm 0.09) \times 10^{-10}$$

The branching fraction for $B^0 \to \mu^+\mu^-$ is smaller than $B_s^0 \to \mu^+\mu^-$ due to the CKM matrix contributions $\frac{|V_{tb}V_{td}^*|^2}{|V_{tb}V_{ts}^*|^2} \sim 0.044$ and larger helicity suppression, therefore although B^0 are produced in greater numbers at the LHC far fewer are observed. This has made the study of $B_s^0 \to \mu^+\mu^-$ a greater priority at the LHCb.

4.4 Current Search Status

The experimental search for dimuon decays began 30 years ago [24] and has continued over the years at different experiments with increasingly sensitive searches producing more and more stringent limits on the branching fractions and recently at the LHC measurements of $\mathcal{B}(B_s^0 \to \mu^+\mu^-)$ [25–33].

Before the LHC the best published limits were $\mathcal{B}(B_s^0 \to \mu^+\mu^-) < 5.1\times10^{-8}$ at 95% confidence level from the D0 experiment [34] using 6.1fb^{-1} of data and from the CDF experiment [35] using 2fb^{-1} data $\mathcal{B}(B^0 \to \mu^+\mu^-) < 1.8^{-8}$ at the 95% confidence level, both limits are consistent with SM predictions. Since the start of data taking at both the LHC the ATLAS, CMS and LHCb detectors have all searched for these decays and LHCb and CMS have made measurements of $\mathcal{B}(B_s^0 \to \mu^+\mu^-)$. The latest results from the LHCb experiment [33] for time integrated branching fractions are

$$\mathcal{B}(B_s^0 \to \mu^+\mu^-) = (2.9^{+1.1}_{-1.0}) \times 10^{-9}$$

$$\mathcal{B}(B^0 \to \mu^+\mu^-) < 7.4 \times 10^{-10} \text{ at } 95\% \text{ C.L.}$$

which are consistent with SM predictions. The $B_s^0 \to \mu^+\mu^-$ signal has significance of 4.0σ. These branching ratios were measured for the combined 2011 and 2012 data set of $1fb^{-1}$ at $\sqrt{s} = 7$ TeV and $2fb^{-1}$ at $\sqrt{s} = 8$ TeV.

The current measurement of $\mathcal{B}(B_s^0 \to \mu^+\mu^-)$ and limit on $\mathcal{B}(B^0 \to \mu^+\mu^-)$ reduces the allowed parameter space for many physics models that describe theories beyond the SM. For example, Fig. 4 illustrates the parameter space for several new physics models which has been significantly reduced by recent measurements, however this does not rule out the models from being true. For many new physics models the most likely branching fractions for $B_s^0 \to \mu^+\mu^-$ and $B^0 \to \mu^+\mu^-$ are very close to the SM prediction however there is also a large likelihood that the branching fraction would be larger than the SM value. Figure 5 shows this likelihood function for $B_s^0 \to \mu^+\mu^-$ for the Non Uniform Higgs Model (NUHM), since the branching fraction for $B_s^0 \to \mu^+\mu^-$ is consistent with the SM value the model is now constrained in its parameter values in the model.

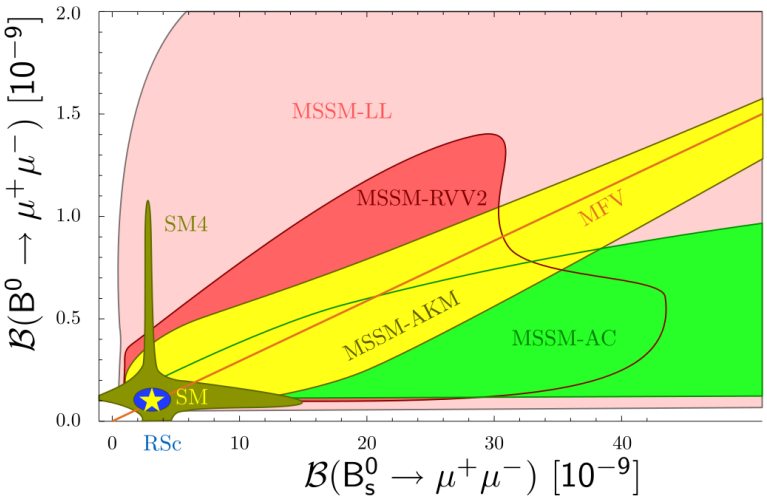

Figure 4: Allowed values for $\mathcal{B}(B_s^0 \to \mu^+\mu^-)$ and $\mathcal{B}(B^0 \to \mu^+\mu^-)$ for Minimal Flavour Violation model (MFV), four super-symmetry flavour models (SUSY) and the SM with a fourth quark generation. The SM value is marked by the star [36]

One New Physics model which is of key interest for future data runs it the Minimal Flavour Violation (MFV) model [37]. The model is an effective field theory and predicts that flavour changes and CP violation beyond the standard model follow known Yukawa couplings. The MFV produces a test for rare decays, though the ratio of their branching fractions [38]

$$\frac{\mathcal{B}(B_s^0 \to \mu^+\mu^-)}{\mathcal{B}(B^0 \to \mu^+\mu^-)} = \frac{f_{B_s^0} m_{B_s^0} |V_{ts}|^2}{f_{B^0} m_{B^0} |V_{tb}|^2} + \mathcal{O}(\frac{m_s}{m_b})$$

where f_B are decay constants and V_{tq} are CKM matrix elements. The prediction for this ratio is shown in Fig. 4 measuring this ratio will give a clear indication of whether or not the MFV could be a correct New Physics theory.

The LHC will begin data taking again in 2015 operating at a center of mass energy of 13 TeV during future data taking periods one aim of the LHCb will be to make a measurement of $\mathcal{B}(B^0 \to \mu^+\mu^-)$ and to improve the significance of the $\mathcal{B}(B_s^0 \to \mu^+\mu^-)$ measurement. A measurement of $\mathcal{B}(B^0 \to \mu^+\mu^-)$ would further reduce the parameter space for new physics models and the ration of the branching fractions would be key in studying the MFV model. In order to the the best branching fraction measurements, improvements to the selection and analysis techniques are being pursued during the LHC downtime.

5 Offline Selection

Selection of events to process is important for data analysis at the LHC. Events that pass the trigger undergo further offline selection cuts before the final data set used for analysis is produced. The offline selection has two different motivations, firstly to reduced the amount of data to a manageable level for the analysis and secondly to cut out as much background from the data as possible whilst keeping a high signal efficiency.

To measure the branching fractions for $B_{(s)}^0 \to \mu^+\mu^-$ two normalisation channels are needed: $B^0 \to K^+\pi^-$ and $B^+ \to J/\psi K^+$. Both decays have well known branching fractions and are used to normalise the number of $B_{(s)}^0 \to \mu^+\mu^-$ events that occur. It is important that the normalisation channels are selected in as similar way as possible to the signal in order to reduce systematic uncertainties in the normalisation process. However some differences in the selection are inevitable because the decays are first selected by different trigger lines.

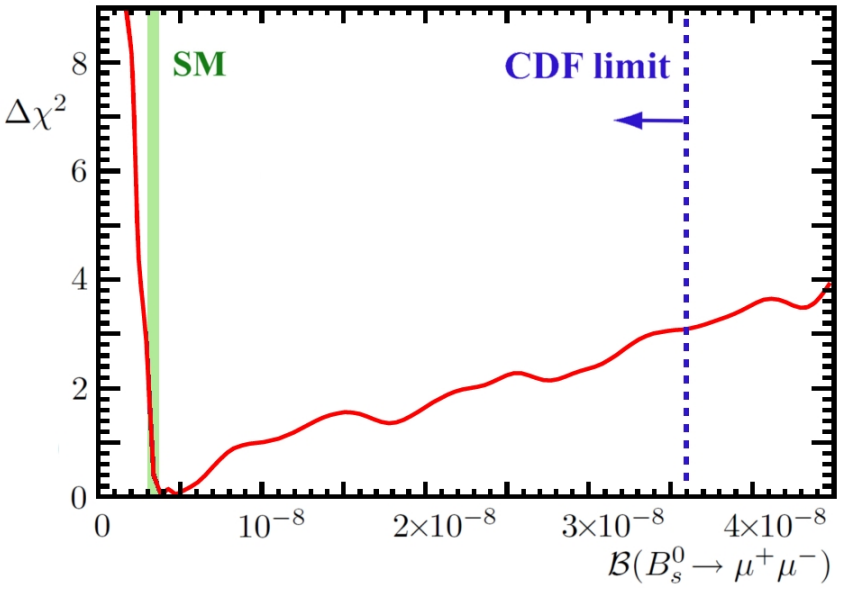

Figure 5: Likelihood function for $\mathcal{B}(B_s^0 \to \mu^+\mu^-)$ for Non Uniform Higgs Model [18]

The first set of cuts that are applied to events passed by the trigger are know at the stripping selection. The stripping selection applies cuts to reconstructed events chosen specifically for each decay. This selection is applied centrally to all events that pass the trigger, only events that pass the stripping selection are then available to be used in the rest of the selection and analysis. Events that do not pass the stripping selection are not lost like those which do not pass the trigger and can be incorporated into the analysis again if stripping cuts change. The selection cuts applied after the stripping are easier to change their focus is less on reducing the amount of data and more focused on reducing the background in the data.

In the run up to the 2015 data taking it is an optimum time to study selection efficiencies, to see where improvements can be make in signal selection efficiencies. This section is focused on improving selection efficiencies by focusing on the stripping lines.

Section 5.1 briefly outlines the $B^0_{(s)} \to \mu^+\mu^-$ selection and stripping efficiencies of the current cuts and Section 5.2 shows studies of improving the efficiencies of the stripping selection.

5.1 Stripping Selection Studies

The stripping cuts were chose by considering three key points:

1. the amount of data allocated to the $B^0_{(s)} \to \mu^+\mu^-$ analysis, originally the order of 10 Hz
2. keeping the selection of signal and normalisation channels as similar as possible
3. the highest possible signal efficiencies taking into account point 1 and 2.

Stripping selection cuts for $B^0_{(s)} \to \mu^+\mu^-$ and $B^+ \to J/\psi K^+$ channels are given in Table 5.1, the same selection applies to $B^0 \to K^+\pi^-$ as for $B^0_{(s)} \to \mu^+\mu^-$. For $B^0_{(s)} \to \mu^+\mu^-$ cuts are applied to the muon impact parameter significance (IPS) and the $B^0_{(s)}$ mass, impact parameter significance (IPS), the distance of flight (DOFS) between the primary and secondary vertices and the track vertex significance. For the normalisation channel $B^+ \to J/\psi K^+$ cuts that are applied to two vertex tracks are applied to the J/ψ rather than the B^+ to that the selection is as similar as possible to that of $B^0_{(s)} \to \mu^+\mu^-$ and there is an additional mass cut on the J/ψ.

Efficiency studies of the stripping selection are based on the study carried out in [39], determining the efficiencies of the stripping cuts on Monte Carlo signal events. An updated version

$B^0_{(s)} \to \mu^+\mu^-$			$B^+ \to J/\psi K^+$		
Particle	Variable	Cut	Particle	Variable	Cut
μ	IP χ^2	> 25	μ	IP χ^2	> 25
			J/ψ	DOFS	> 15
				vertex χ^2	< 9
				$\mid M_{\mu^+\mu^-} - M_{J\psi,PGD} \mid$	< 60 MeV/c^2
$B_{(s)}$	$\mid M - M_{B,PGD} \mid$	< 600 MeV/c^2	B^+	$\mid M - M_{B,PGD} \mid$	< 600 MeV/c^2
	IP χ^2	< 25		IP χ^2	< 25
	DOFS	> 15			
	vertex χ^2	< 9			

Table 1: Table of stripping selection cuts. DOFS is the Distance of Flight Significance and IPS is Impact Parameter Significance.

of the study has been carried out to check whether the efficiencies are the same for the current cuts given that new Monte Carlo data has been produced and also to allow further study into efficiency improvements in the stripping selection. Furthermore for the 2015 running of the LHC different storage methods will be in place allowing a greater amount of data to be stored for the decay therefore higher efficiencies can be used.

The efficiencies for current stripping cuts have been calculated using Sim06b-MC2012 simulation, with Pythia 6. A very loose stripping applied has been applied to events and no trigger requirements were imposed. Table 5.1 shows the efficiencies for the stripping selection cuts for the signal and normalisation channel. The DOFS cut and the IPS cut for the muons are the least efficient cuts and hence areas for efficiency improvements.

Fig. 6 shows the ratio of the signal for $B_s \to \mu^+\mu^-$ to normalisation channel for a range of different stripping cut values. For cuts on the $B^0_{(s)}$ the ratio of efficiencies is very close to 1, within 4% for a large range of cut values which adheres to the second criteria mentioned for defining the stripping selection. The ratio of the signal and normalisation channels for the daughter particle IPS markedly deviates from unity, showing that the IPS distribution of the muons and kaon are very different.

Stripping cut	$B_s \to \mu^+\mu^-$	$B_d \to \mu^+\mu^-$	$B^+ \to J/\psi(\mu^+\mu^-)K^+$
$\mid M - M_{B,PGD} \mid < 600$ MeV	98.59	98.72	99.86
B, J/ψ vertex $\chi^2 < 9$	97.21	97.18	96.78
B IPS < 5	96.78	96.93	97.52
DOFS(B,J/ψ)> 15	83.74	83.96	82.90
Minimum IPS$(\mu^+, \mu^-) > 5$	80.16	80.62	86.98
K^+ IPS > 5			
$\mid M(\mu^+\mu^-) - M_{J/\psi,PGD} \mid < 60$ MeV	-	-	96.47
Total	$70.82 \pm 0.07\%$	$71.35 \pm 0.07\%$	$69.36 \pm 0.19\%$

Table 2: Table of stripping selection efficiencies for current stripping selection cuts.

5.2 Improvement studies

The selection requirements on DOFS and IPS for the muons have the lowest efficiencies of all the stripping cuts and increases of stripping efficiencies could be found here. Figure 7 shows the total efficiencies after all the stripping cuts have been applied for a range of DOFS and daughter IPS cut values. In order to improve the overall efficiency of the stripping selections both cut

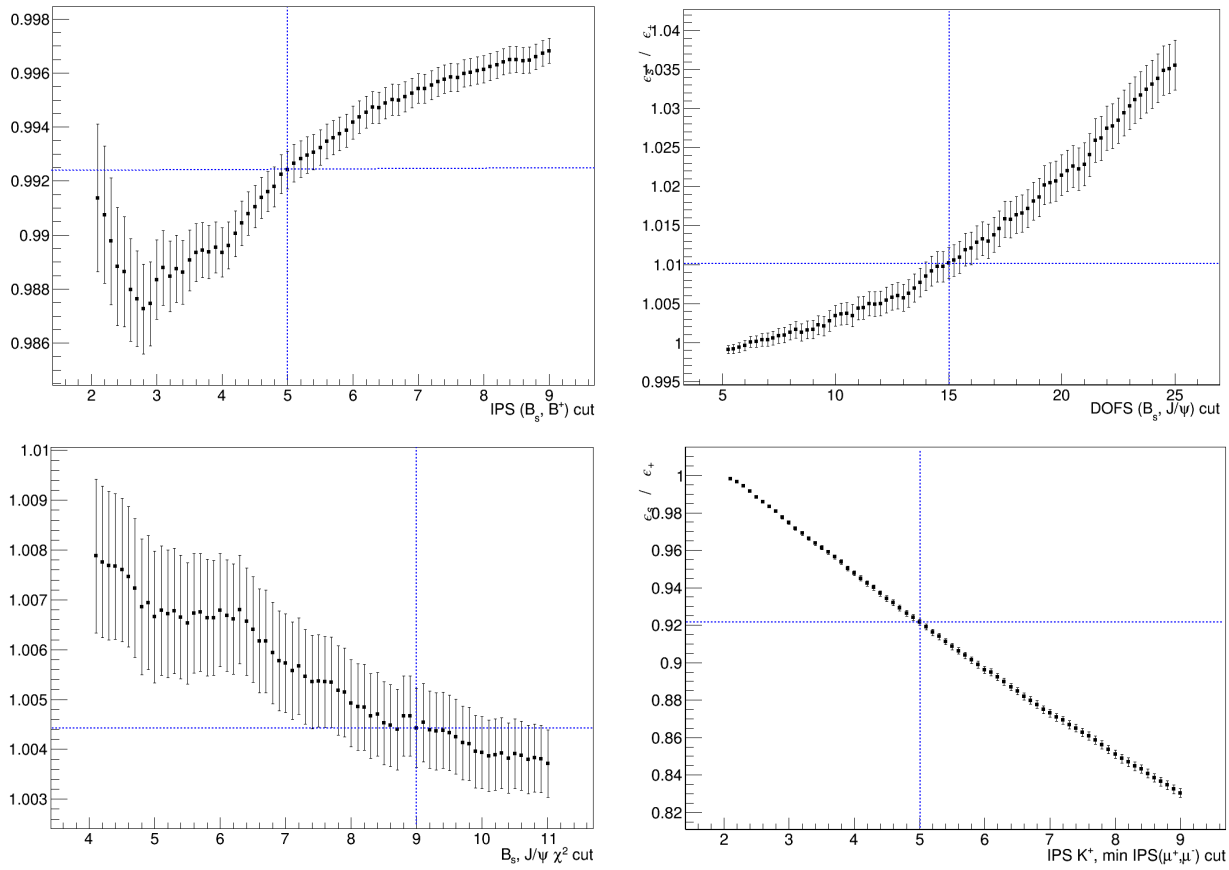

Figure 6: Ratio plots for different cuts where the blue lines mark the current cut value.

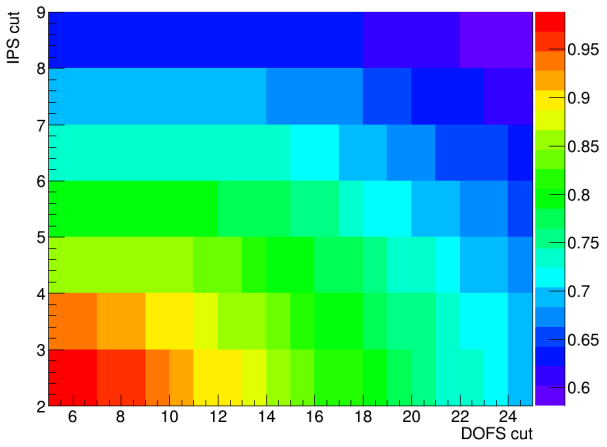

Figure 7: Efficiency after stripping cuts for a range of $B^0_{(s)}$ distance of flight and muon impact parameter significance cut values.

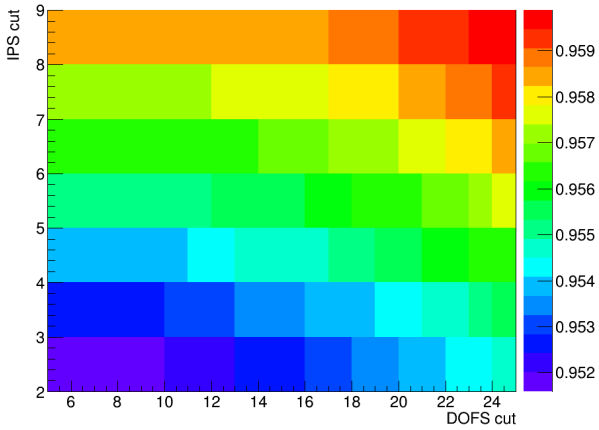

Figure 8: Trigger efficiencies of events which pass the stripping cuts for a range of $B^0_{(s)}$ distance of flight and muon impact parameter significance cut values.

values need to be lowered, to see much improvement in efficiency the daughter IPS cuts must be loosened by more than the DOFS cut. The events gained by increasing the stripping selection efficiency improvements must also pass the trigger requirements in order to make a change on the final analysis. Figure 8 shows the trigger efficiencies on events that have passed all the stripping cuts for the range of DOFS and daughter IPS cut values used in figure 7. It is clear that all efficiency gains made in the stripping selection will not be lost in the trigger.

In previous analyses the amount of data that can pass the stripping selection has been limited to 10 Hz. Although this limit will be increased for future analyses it will not be limitless. Therefore any loosening of stripping cuts that improves the efficiencies must take into account the amount of data retained by the cuts. Tables 3, 4 and 5 show data retentions for signal and normalisation channels. The amount of data kept with the current cut values for DOFS and daughter IPS have been normalised to 1 so that the increase in data kept as the cuts are loosened is clear. An increase of 16% in signal efficiency would create 6.5 times the current amount of data kept for the signal channel and the amount of data kept for the normalisation channels would increase too though by not as much. This study has given an insight as to where efficiency can be gained in the stripping selection, however further studies need to be performed in order to determine which cut values would be optimum to use, this would need to take into account more specific details on how much data should pass the stripping lines so that a manageable amount of data was kept.

DOFS cut	IPS(μ^+, μ^-)	Fractional Increase	Efficiency of cuts
15	5.00	1	70.8
14	4.25	1.32	74.4
13	4.00	1.66	76.3
12	3.50	2.46	79.2
11	3.00	3.60	82.1
10	2.75	4.88	84.2
9	2.50	6.90	86.3

Table 3: Retention of data for $B^0_{(s)} \to \mu^+\mu^-$ for a range of DOFS and muon IPS cuts. Fractional increase is the increase in data retention as the cut values change where the current cut value is normalised to 1.

DOFS cut	IPS(K^+, π^-)	Fractional Increase	Efficiency of cuts
15	5.00	1.00	71.3
14	4.25	1.22	74.9
13	4.00	1.40	76.9
12	3.50	1.83	79.8
11	3.00	2.51	82.8
10	2.75	3.23	85.0
9	2.50	4.19	87.2

Table 4: Retention of data for $B^0 \to K^+\pi^-$ for a range of DOFS and muon IPS cuts. Fractional increase is the increase in data retention as the cut values change where the current cut value is normalised to 1.

DOFS cut	IPS K^+	Fractional Increase	Efficiency of cuts
15	5.00	1.00	69.4
14	4.25	1.05	72.6
13	4.00	1.10	74.6
12	3.50	1.16	77.3
11	3.00	1.22	80.1
10	2.75	1.28	82.1
9	2.50	1.35	84.3

Table 5: Retention of data for $B^+ \to J/\psi K^+$ for a range of DOFS and muon IPS cuts. Fractional increase is the increase in data retention as the cut values change where the current cut value is normalised to 1.

6 Mass Reconstruction and Resolution

Accurate invariant mass reconstruction is important for event analysis at the LHC. For $B^0_{(s)} \to \mu^+\mu^-$ studies good mass resolution is necessary to separate the B^0 and B^0_s mesons and to separate background from $B \to h^+h^-$ events where the hadrons are mis-identified as muons. This section looks at the impact of using two different methods for constructing the invariant mass of decays in the $B^0_s \to \mu^+\mu^-$ analysis. The effects of using a different decay fitter, decay tree fitter, and including a momentum scaling correction are studied.

Section 6.1 outlines how the fitter and scaling works and Section 6.2 studies then impact of using them on the reconstructed mass resolution.

6.1 Decay Tree Fitter and Momentum Scaling

Decay tree fitter (DTF) is a fitting tool that is used to reconstruct particle decays [40], it was developed for use at BaBar to reconstruct $K^0_S \to \pi^0\pi^0$ decays, amongst others. For a decay such as $B^0 \to J/\psi(\mu\mu)K^0_s(\pi\pi)$ most fitters will reconstruct the K^0_s from the pions and the J/ψ from the muons first and then construct the B from the J/ψ and K^0_s. DTF is different, it reconstructs the whole decay in one step taking into account both mass and vertex imposed constraints. This method can lead get better mass resolutions and a more constrained fit.

Momentum scaling can be used before event reconstruction to take into account QED radiative corrections [41], if radiative corrections are not correctly accounted for then the loss in energy from radiation will cause a lower reconsturct ed mass than expected. On order to account for this a momentum scale has been formulated. The scale was developed for $J/\psi \to \mu^+\mu^-$ decays, the mass peak for the decay was reconstructed and the mean compared to the expected peak mean. A scaling factor α was calculated so that the measured mean equals the reconstructed mean when multiplied by $(1-\alpha)$. The value for α was then checked across a series of decays.

Momentum scaling can be used in event reconstruction to improve the accuracy of mass reconstruction, however due to the way in which the implementation procedure was developed it must be used in conjunction with Decay Tree Fitter.

6.2 Resolution Improvements

The decays $B \to K^\pm\pi^\mp$, $B^+ \to \mathrm{J}/\psi\ K^+$ and $B_s \to \mathrm{J}/\psi\ \phi$ were used to study the effect of momentum scaling and DTF on the mass resolution, these decays produce clear mass peaks necessary from the study of mass resolutions. A comparison of mass reconstruction using momentum scaling and DTF with the previous reconstruction methods is shown in Figure 9. The signal has been fitted a Gaussian functions with a power law tail at the low mass side and the background has been fitted with an exponential. The fits do not model the background in the data sample particularly well however since it is improvements to the resolution of the peak is of interest here the background fit is unimportant. The effects of momentum scaling and decay tree fitter are small however it can be seen from the plots that there is a downward shift in the peak mean closer to the expected B meson mass and the peaks are narrower when the scaling is included. This is highlighted in table 6. Overall there is between $1-3\%$ improvement in mass resolution and the mass peak mean is shifted closer to the expected B-hadron mass.

Although the improvements in the mass resolution are small they show a consistent improvement for all of the decays studied, therefore momentum scaling and decay tree fitter should be included into the reconstruction of $B^0_s \to \mu^+\mu^-$ analysis.

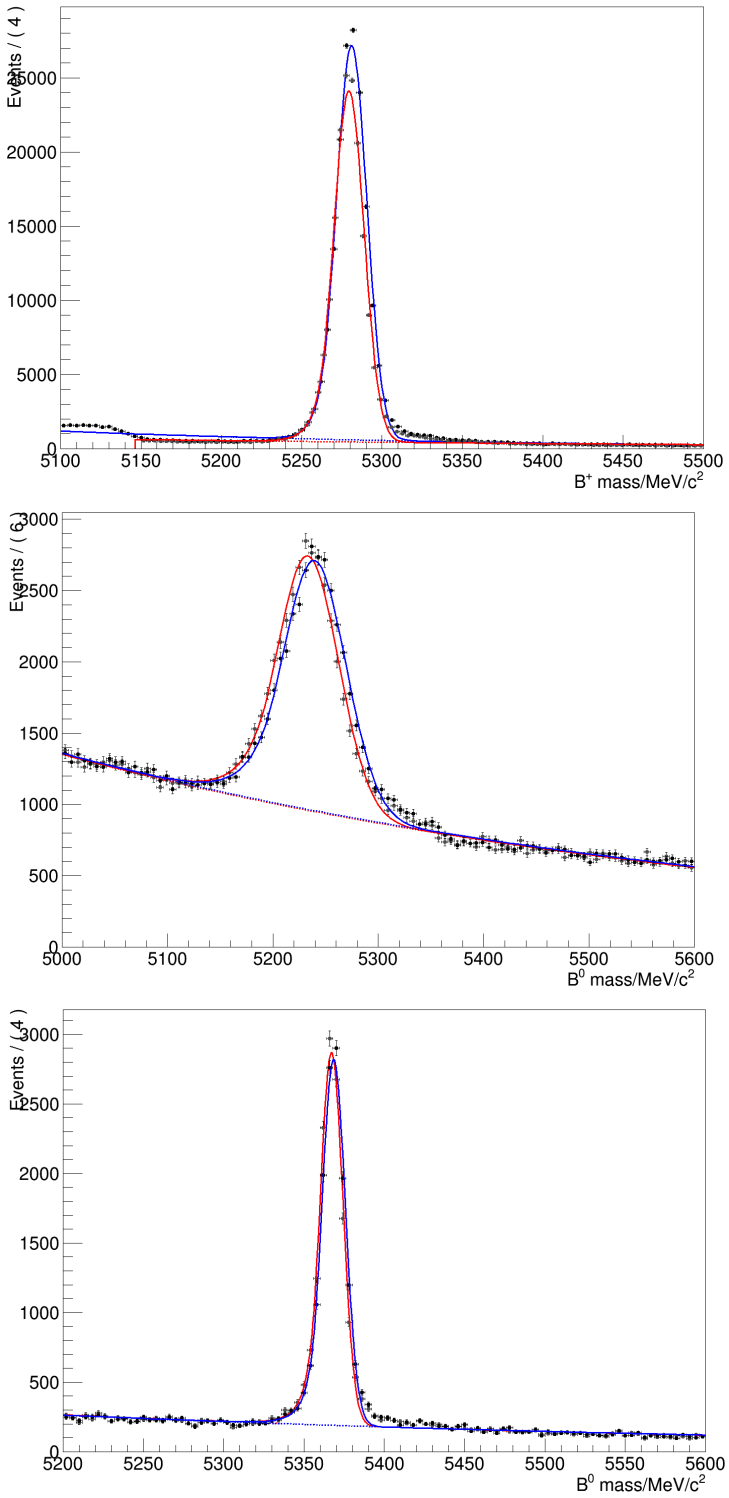

Figure 9: Mass fits of data with and without momentum scaling, where grey data points and the red fit are for momentum scaling and DTF and black data points and the blue fit are the previous reconstruction method. The signal has been fitted a Gaussian functions with a power law tail at the low mass side and the background has been fitted with an exponential. Decays on order from top to bottom are $B^+ \to \mathrm{J}/\psi\ K^+$, $B \to K^{\pm}\pi^{\mp}$ and $B_s \to \mathrm{J}/\psi\ \phi$.

Decay	μ [MeV/c^2]	σ [MeV/c^2]
Without Scaling		
$B \to K^{\pm}\pi^{\mp}$	5239.5	29.8
$B^+ \to \mathrm{J}/\psi\ K^+$	5281.00	9.51
$B_s \to \mathrm{J}/\psi\ \phi$	5368.42	7.26
With Scaling		
$B \to K^{\pm}\pi^{\mp}$	5233.2	29.1
$B^+ \to \mathrm{J}/\psi\ K^+$	5279.36	9.39
$B_s \to \mathrm{J}/\psi\ \phi$	5367.10	7.07

Table 6: Width and mean of mass fits both with and without momentum scaling and DTF.

7 Summary

This report has focused on improving two different aspects of the $B_s \to \mu^+\mu^-$ branching fraction analysis. Studies of the stripping selection for $B_s \to \mu^+\mu^-$ events has shown that significant efficiency improvements can be made there, however the about of data retained by the stripping selection must be taken into account before new cut values can be fixed. Defining the stripping selection is import for the next data taking period, the selection chosen will then be used for several years therefore it is important that the selection is studies thoroughly before it is finalised.

Mass resolution studies have revealed that including momentum scaling and using DTF reconstruction tool improves the mass resolution by $1-3\%$. The data from 2011 and 2012 runs will be re-analysed with the improvements from DTF and momentum scaling included and they will also be incorporated in future analyses.

Further improvements to signal efficiencies can be gained by considering improvements in other offline cuts [42]. In particular looking at the cut to reduce low p_t background from exclusive dimuon production from $pp \to p\mu^+\mu^- p$ decays. This background motivated a low p_t cut on the B-hadron of $B_{p_t} > 500$ MeV to be used however studies have shown that this cut could be loosened [43], which would the effect the selection efficiencies.

References

[1] Lyndon Evans and Philip Bryant. LHC Machine. *JINST*, 3:S08001, 2008.

[2] G. Aad et al. The ATLAS Experiment at the CERN Large Hadron Collider. *JINST*, 3:S08003, 2008.

[3] S. Chatrchyan et al. The CMS experiment at the CERN LHC. *JINST*, 3:S08004, 2008.

[4] Georges Aad et al. Observation of a new particle in the search for the Standard Model Higgs boson with the ATLAS detector at the LHC. *Phys.Lett.*, B716:1–29, 2012.

[5] Serguei Chatrchyan et al. Observation of a new boson at a mass of 125 GeV with the CMS experiment at the LHC. *Phys.Lett.*, B716:30–61, 2012.

[6] K. Aamodt et al. The ALICE experiment at the CERN LHC. *JINST*, 3:S08002, 2008.

[7] Jr. Alves, A. Augusto et al. The LHCb Detector at the LHC. *JINST*, 3:S08005, 2008.

[8] B. Adeva et al. Roadmap for selected key measurements of LHCb. 2009.

[9] S.K. Choi et al. Observation of a resonance-like structure in the pi+- psi-prime mass distribution in exclusive $B \to Kpi + -psi - prime$ decays. *Phys.Rev.Lett.*, 100:142001, 2008.

[10] Roel Aaij et al. Observation of the resonant character of the $Z(4430)^-$ state. *Phys.Rev.Lett.*, 112:222002, 2014.

[11] S. Fukuda et al. Constraints on neutrino oscillations using 1258 days of Super-Kamiokande solar neutrino data. *Phys.Rev.Lett.*, 86:5656–5660, 2001.

[12] Y. Fukuda et al. Measurements of the solar neutrino flux from Super-Kamiokande's first 300 days. *Phys.Rev.Lett.*, 81:1158–1162, 1998.

[13] Jr. Davis, Raymond, Don S. Harmer, and Kenneth C. Hoffman. Search for neutrinos from the sun. *Phys.Rev.Lett.*, 20:1205–1209, 1968.

[14] Roberts and Rots. Comparison of Rotation Curves of Different Galaxy Types. *Astronomy and Astrophysics*, 26:483–485, aug 1973.

[15] F. Zwicky. Die Rotverschiebung von extragalaktischen Nebeln. *Helv.Phys.Acta*, 6:110–127, 1933.

[16] Zwicky. On the Masses of Nebulae and of Clusters of Nebulae. *Astrophys. J.*, 86:217, oct 1937.

[17] J. Beringer et al. Review of Particle Physics (RPP). *Phys.Rev.*, D86:010001, 2012.

[18] Marc-Olivier Bettler and O Schneider. *Construction of the Inner Tracker and Sensitivity to the $B_s^0 \to \mu\mu$ Decay at LHCb*. PhD thesis, LPHE, Lausanne, Lausanne, 2010. Presented 01 Apr 2010.

[19] Kenneth G. Wilson. Nonlagrangian models of current algebra. *Phys.Rev.*, 179:1499–1512, 1969.

[20] K.G. Wilson and W. Zimmermann. Operator product expansions and composite field operators in the general framework of quantum field theory. *Commun.Math.Phys.*, 24:87–106, 1972.

[21] Andrzej J. Buras. Weak Hamiltonian, CP violation and rare decays. pages 281–539, 1998.

[22] C. Bobeth, T. Ewerth, F. Kruger, and J. Urban. Analysis of neutral Higgs boson contributions to the decays $\bar{B}(\ s^{)} \to \ell^+\ell^-$ and $\bar{B} \to K\ell^+\ell^-$. *Phys.Rev.*, D64:074014, 2001.

[23] Christoph Bobeth, Martin Gorbahn, Thomas Hermann, Mikolaj Misiak, Emmanuel Stamou, et al. $b_{s,d} \to l^+l^-$ in the standard model with reduced theoretical uncertainty. *Phys.Rev.Lett.*, 112:101801, 2014.

[24] T. Bergfeld et al. Search for decays of B^0 mesons into pairs of leptons: $B^0 \to e^+e^-$, $B^0 \to$ muon+ muon- and $B^0 \to e^\pm$ muon-+. *Phys.Rev.*, D62:091102, 2000.

[25] S. "Chatrchyan and others". "measurement of the bs0→μ+μ- branching fraction and search for b0→μ+μ- with the cms experiment". *"Phys. Rev. Lett."*, "111":"101804", "Sep" "2013".

[26] C. Albajar et al. A search for rare b meson decays at the cern spps collider. *Physics Letters B*, 262(1):163 – 170, 1991.

[27] Georges Aad et al. Search for the decay Bs0 -¿ mu mu with the ATLAS detector. *Phys.Lett.*, B713:387–407, 2012.

[28] Victor Mukhamedovich Abazov et al. Search for the rare decay $B_s \to \mu\mu$. *Phys.Rev.*, D87(7):072006, 2013.

[29] T. Aaltonen et al. Search for $B_s \to \mu^+\mu^-$ and $B_d \to \mu^+\mu^-$ decays with the full CDF Run II data set. *Phys.Rev.*, D87:072003, 2013.

[30] B. "Aubert and others". "search for decays of b0 mesons into e+e-, $\mu^+\mu^-$ and $e^+\mu^-$ final states". *"Phys. Rev. D"*, "77":"032007", "Feb" "2008".

[31] M.C. Chang et al. Search for $B^0 \to \ell^+\ell^-$ at BELLE. *Phys.Rev.*, D68:111101, 2003.

[32] H. Albrecht et al. B meson decays into charmonium states. *Physics Letters B*, 199(3):451 – 456, 1987.

[33] R. Aaij et al. Measurement of the $B_s^0 \to \mu^+\mu^-$ branching fraction and search for $B^0 \to \mu^+\mu^-$ decays at the LHCb experiment. *Phys.Rev.Lett.*, 111:101805, 2013.

[34] Victor Mukhamedovich Abazov et al. Search for the rare decay $B_s^0 \to \mu^+\mu^-$. *Phys.Lett.*, B693:539–544, 2010.

[35] T. Aaltonen et al. Search for $B_s^0 \to \mu^+\mu^-$ and $B_d^0 \to \mu^+\mu^-$ decays with $2fb^{-1}$ of $p\bar{p}$ collisions. *Phys.Rev.Lett.*, 100:101802, 2008.

[36] David M. Straub. Overview of Constraints on New Physics in Rare B Decays. 2012.

[37] G. D'Ambrosio, G.F. Giudice, G. Isidori, and A. Strumia. Minimal flavor violation: An Effective field theory approach. *Nucl.Phys.*, B645:155–187, 2002.

[38] Tobias Hurth, Gino Isidori, Jernej F. Kamenik, and Federico Mescia. Constraints on New Physics in MFV models: A Model-independent analysis of Δ F = 1 processes. *Nucl.Phys.*, B808:326–346, 2009.

[39] D Martinez Santos, B Adeva Andany, and J A Hernando Morata. *Study of the very rare decay $B_s \to \mu^+\mu^-$ in LHCb*. PhD thesis, Santiago de Compostela, Universidade de Santiago de Compostela, Santiago de Compostela, 2010. Presented on 05 May 2010.

[40] Wouter D. Hulsbergen. Decay chain fitting with a Kalman filter. *Nucl.Instrum.Meth.*, A552:566–575, 2005.

[41] R. Aaij et al. Measurement of b-hadron masses. *Phys.Lett.*, B708:241–248, 2012.

[42] C Adrover, J Albrecht, F Archilli, M-O Bettler, X Cid Vidal, F Dettori, C Elsasser, J A Hernando Morata, G Lanfranchi, G Mancinelli, D Martinez Santos, M Palutan, M Perrin-Terrin, N Sagidova, A Sarti, B Sciascia, J Serrano, F Soomro, Y Shcheglov, and O Steinkamp. Search for the rare decays $B_s^0 \to \mu^+\mu^-$ and $B^0 \to \mu^+\mu^-$ with 1.02 fb $^{-1}$. Mar 2012.

[43] Roel Aaij et al. Updated measurements of exclusive J/ψ and ψ(2S) production cross-sections in pp collisions at $\sqrt{s} = 7$ TeV. *J.Phys.*, G41:055002, 2014.